# Experimental Implementation of an Enhanced Field Oriented Control Strategy for Induction Motors Using a Low-Cost ATSAM3X8E Microcontroller

M. Caruso, A. O. Di Tommaso, R. Miceli, *Member, IEEE,* C. Nevoloso and G. Vassallo
Department of Engineering, University of Palermo
Viale delle Scienze, Building nr. 9, 90128 - Palermo, Italy
Email: massimo.caruso16@unipa.it

***Abstract*—This paper presents a low-cost Micro Controller Unit (MCU) implementation of an enhanced Field Oriented Control (FOC) technique that takes into account the non-linearity of the ferromagnetic material. The algorithm is applied to a three-phase 5.5 kW Induction Motor (IM) and experimentally carried out by means of an ATMEL ATSAM3X8E microcontroller. The effectiveness of the enhanced control strategy is verified by comparing the dynamic performances of the electric drive with those obtained by means of a traditional FOC technique. For this purpose, an experimental test bench is set up for the implementation of the enhanced FOC technique. Finally, the technical and economic features of the simple and flexible implementation by means of the proposed microcontroller are discussed and compared with traditional ones, demonstrating the fact that the adopted system can be successfully adopted for high-performance electric drive applications.**

***Index Terms*—Field Oriented Control (FOC), microcontroller, induction motors, electrical drives.**

## I. Introduction

Over the last years, the electrical drives (EDs) for induction motors have reached great interest due to their relevant technical improvement in terms of flexibility, robustness and accuracy. These drives are applied in a very wide range of industry and automotive applications, such as traction drives and railways [1]–[11]. Thus, the related scientific research has dedicated the efforts towards the conception of innovative, more accurate and low-cost MCU control techniques, capable of enhancing the performance of the whole drive, decreasing, at the same time, the overall costs [12]. As for the technical improvements, the exact determination of the IM parameters is crucial for a more efficient drive: indeed, these parameters can considerably change with the frequency (mainly for the core loss resistance), saturation (mainly for the core reactance) and temperature (mainly for the rotor resistance) [13]–[19]. Therefore, the traditional Field Oriented Control (FOC) technique, which is very widely applied in the field of EDs, can be enhanced with a real-time estimation of the previously mentioned parameters. As for the economical aspects, it can be stated that the costs of recent microcontrollers have been significantly reduced if compared with their older analog versions [20]–[23]. The market in this field offers a wide choice of microcontrollers, such as DSPs (Digital Signal Processors), FPGAs (Field Programmable Gate Arrays), or Complex Programmable Logic Devices (CPLDs), which are also equipped with all the peripherals needed for electric drive applications, such as PWM and encoder units, communication ports, analog-to-digital and digital-to-analog converters, etc. A good compromise between technical performance and cost is represented by the ATMEL ATSAM3X8E microcontroller, whose features will be widely discussed in the next Sections.

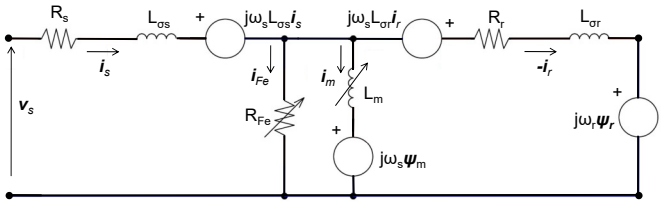


Figure 1. The IM equivalent circuit.

In this context, this work presents a low-cost MCU implementation of an enhanced FOC algorithm that considers the non-linearity of the ferromagnetic material. This technique is applied to a 5.5 kW IM and experimentally implemented through a flexible ATMEL ATSAM3X8E microcontroller. The experimental results are compared with those obtained by means of a traditional FOC technique, highlighting also the technical and economic advantages of the adopted microcontroller.

More specifically, this work is organized as follows: Section II describes the equations representing the enhanced FOC technique, which is experimentally implemented by means of the test bench equipment discussed in Section III. The experimental results are reported in Section IV, whereas the technical and economic features of the adopted microcontroller are investigated in Section V.

## II. The Enhanced FOC Technique

In this Section, the equations governing the FOC algorithm are briefly presented. The proposed enhanced strategy is obtained by considering an improved machine model (see Fig. 1), expressed in the synchronous rotating reference frame, which considers the core saturation effects of the ferromagnetic material.

More in particular, by imposing the rotor flux oriented control condition

$$\frac{d\psi_{rq}}{dt} = \psi_{rq} = 0, \tag{1}$$

978-1-7281-5641-5/20/$31.00©2020 European Union

the model is described by the following equations:

$$T_{\sigma r}\frac{d\psi_{rd}}{dt}+\psi_{rd}=\psi_{md}, \tag{2}$$

$$\omega_s=\frac{d\theta_s}{dt}=\frac{T_{\sigma r}}{\psi_{mq}}\psi_{rd}+\omega_r, \tag{3}$$

$$T_{\sigma Fe}\frac{d\psi_{md}}{dt}+\psi_{md}=L_{\sigma r}\left(i_{sd}-i_{md}\right)+\psi_{rd}+T_{\sigma Fe}\omega_s\psi_{mq}, \tag{4}$$

$$T_{\sigma Fe}\frac{d\psi_{mq}}{dt}+\psi_{mq}=L_{\sigma r}\left(i_{sq}-i_{mq}\right)-T_{\sigma Fe}\omega_s\psi_{md}, \tag{5}$$

where $\psi_{rd}$ and $\psi_{rq}$ are the direct-axis and quadrature-axis rotor flux components and $\psi_{md}$ and $\psi_{mq}$ are the direct-axis and quadrature-axis magnetizing flux components, respectively, $\omega_r$ and $\omega_s$ represent the rotor speed and the synchronous speed, $i_{sd}$ and $i_{sq}$ are the direct-axis and quadrature-axis stator current components, respectively. Moreover, two rotor time constants $T_{\sigma r}={}^{L_{\sigma r}}/_{R_r}$ and $T_{\sigma Fe}={}^{L_{\sigma r}}/_{R_{Fe}}$ are defined, where $R_{Fe}$ is the core loss resistance, $R_r$ and $L_{\sigma r}$ are the rotor resistance and the rotor leakage inductance, respectively. The direct-axis and quadrature-axis magnetizing current components, namely $i_{md}$ and $i_{mq}$, can be determined as

$$i_{md}=i_m\frac{\psi_{md}}{\psi_m} \tag{6}$$

and

$$i_{mq}=i_m\frac{\psi_{mq}}{\psi_m}, \tag{7}$$

where

$$\psi_m=\sqrt{\psi_{md}^2+\psi_{mq}^2}. \tag{8}$$

If saturation of the magnetic circuit is neglected, the magnetizing current is calculated as $i_m={}^{\psi_m}/_{L_m}$, where $L_m$ is the magnetizing inductance, otherwise magnetic saturation is taken into account by introducing the IM magnetizing characteristic $i_m=f(\psi_m)$.

The electromagnetic torque $T_{em}$ can be expressed as function of the magnetizing flux components ($p$ is the number of pole pairs):

$$T_{em}=\frac{3}{2}p\frac{1}{L_{\sigma r}}\psi_{md}\psi_{mq}=K_T\psi_{md}\psi_{mq}. \tag{9}$$

As aforementioned, for a more accurate model, the variation of the magnetizing reactance with saturation should be considered, instead leakage reactances are not highly affected by this phenomenon [19]. Thus, the core saturation is taken into account by considering the magnetizing curve $i_m=f(\psi_m)$ depicted in Fig. 2, which has been experimentally obtained by means of a no-load test at synchronous speed. The equation that fits the related trend is given by (see Fig. 2):

$$\begin{aligned} i_m=&\,119.6\psi_m^6+250.8\psi_m^5+181.7\psi_m^4\\ &-44.92\psi_m^3-0.83\psi_m^2+4.43\psi_m. \end{aligned} \tag{10}$$

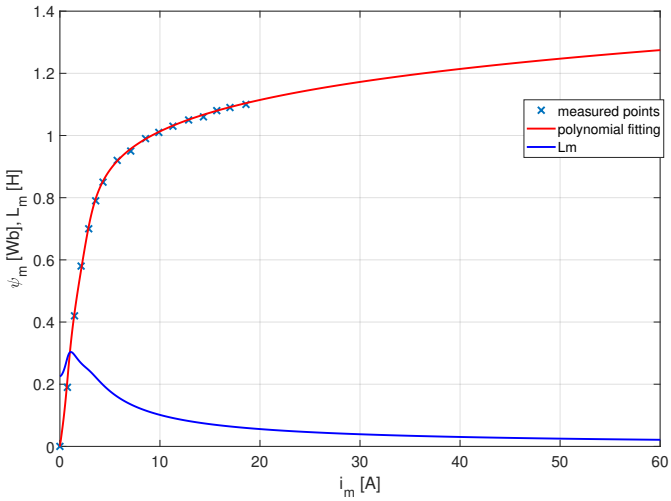


Figure 2. Magnetizing curve and actual trend of the magnetizing inductance $L_m$.

The simplified FOC block scheme, which implements (1-10), is shown in Fig. 3. In the torque control channel, the output IM position is compared with the reference position $\theta_{ref}$ and the error is processed by a PI controller in order to provide the reference speed $\omega_{ref}$, which is, then, compared with the IM output speed. The speed error is processed by the PI, providing the reference $q$-axis current, $i_{sq}^*$, which is compared with the $i_{sq}$ current of the motor. The determined error provides the reference $q$-axis voltage $v_{sq}^*$, needed for the motor supply. In the magnetization control channel, the reference flux is compared with the IM rotor flux. The error processed by the PI provides the reference direct-axis current component, $i_{sd}^*$, and the current of the IM, namely $i_{sd}$, determines the reference $d$-axis voltage $v_{sd}^*$. Finally, the decoupled $v_{sd}^*$ and $v_{sq}^*$ signals are sent to the Space Vector Modulation block, providing the input quantities for the inverter.

The implementation of the reference frame transformations, the PI controllers and the space vector modulation is deeply discussed in [24].

## III. Test Bench Equipment

The experimental implementation of the control strategy is performed by means of the test bench shown in Fig. 2 (a-b). It is mainly composed by:

- A 5.5 kW three-phase, double squirrel-cage, induction motor, whose rated speed and rated current are equal to 3000 rpm and 13 A, respectively, depicted in Fig. 5 and whose main rated values and electrical quantities are summarized in Table I.
- A SINUS-IFDE digital power converter (Elettronica Santerno Inc.), which drives the IM by adopting a Space Vector Pulse Width Modulation technique (the switching frequency is equal to 10 kHz). The main features are summarized in Table II.
- A Direct Current Machine (Stipaf Elettromeccanica), whose rated power and rated current are equal to 7.8 kW and 22.5 A, respectively, adopted as a mechanical load for the induction motor.

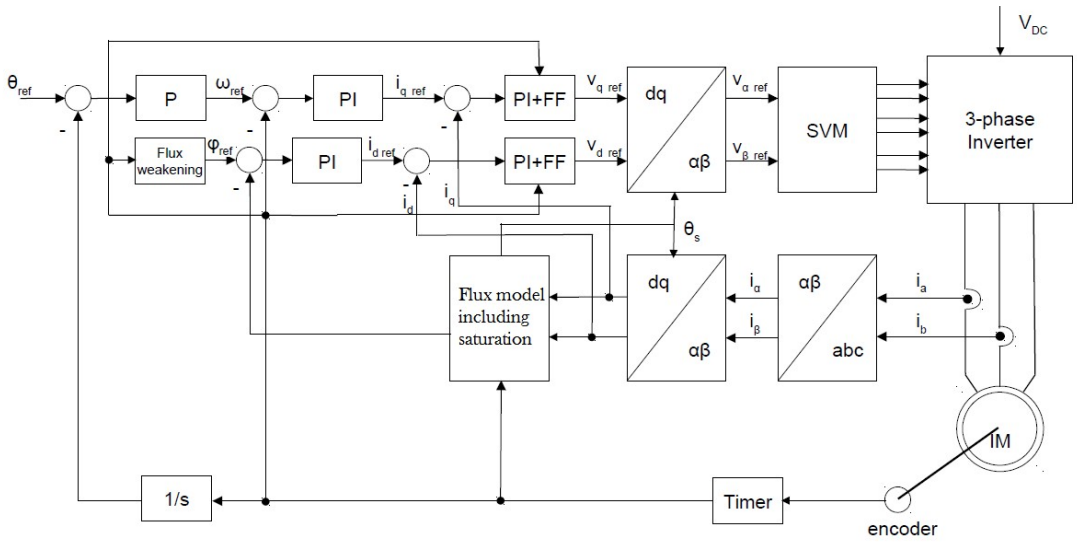


Figure 3. Block scheme of the enhanced FOC for a three-phase induction motor.

Table I
MAIN RATED VALUES AND PARAMETERS OF THE IM UNDER TEST.

| Quantity | Value |
|---|---|
| Power [kW] | 5.5 |
| Voltage [V] | 400 |
| Current [A] | 13 |
| Frequency [Hz] | 50 |
| Torque [Nm] | 18 |
| Rated speed [rpm] | 2850 |
| Stator resistance [Ω] | 0.56 |
| Rotor resistance [Ω] | 0.77 |
| Stator inductance [H] | 0.116 |
| Rotor inductance [H] | 0.119 |
| $k_1$ [$\Omega\, s$] | 2.75 |
| $k_2$ [$\Omega\, s^2$] | 0.141 |
| Rated rotor flux [Wb] | 0.7 |

Table II
DATA OF THE SINUS-IFDE INVERTER.

| Parameter | Value |
|---|---|
| Input voltage [V] | 380...460 |
| Input frequency [Hz] | 50/60 |
| Input current [A] | 35 |
| Output power [kVA] | 21.1 |
| Output voltage [V] | 0...380...460 |
| Output current [A] | 32 |
| Output frequency [Hz] | 0...800 |

- An optical incremental encoder (Eltra Inc., model EH80), used for the rotor speed detection.
- A CRM90.40 rectifier (Elettronica Santerno), directly connected to the electrical grid, used to drive the DC machine.
- A dSPACE control board, used for the real-time supervision and control of the electromagnetic torque generated by the DC machine.
- A three-phase PZ4000 power analyzer (Yokogawa Inc.) for the real-time measurement and acquisition of voltage, current and active power.
- An ATMEL ATSAM3X8E microcontroller (type ARM), mounted on an "Arduino Due" board, running at a clock frequency of 84 MHz and used for the implementation of the enhanced FOC strategy. Moreover, a compatible Arduino shield, which is shown in Fig. 6, has been adequately designed and realized in order to easily connect the microcontroller board with the inverter. Furthermore, the conditioning circuits of the current sensors, shown in Fig. 7, are contained within the shield.

## IV. EXPERIMENTAL RESULTS

This Section discusses the experimental results obtained from the implementation of the enhanced FOC algorithm and compares the dynamic performances of the drive with those obtained through a FOC without considering the main flux saturation.

More in detail, Fig. 8a shows the trends over time of direct-axis and quadrature axis voltage components (red and orange lines, respectively) and DC link voltage (blue line) during multiple speed variations from 400 rpm to -400 rpm at no load conditions. For the same working conditions, Fig. 8b plots the experimental results obtained with the FOC algorithm without considering the main flux saturation. Moreover, the trends of the synchronous speed and rotor speed for both algorithms are reported in Figs. 9a and 9b, respectively. From this plots and from Fig. 10, which shows the comparison of the dynamic responses of the two algorithms, it can be noticed that the implementation of the enhanced FOC algorithm provides a better dynamic response.

Other significant results can be observed in Figs. 11 and 11b, which plot the profiles of the direct-axis and quadrature-axis current components for both algorithms during multiple acceleration/deceleration tests from -300 rpm to +300 rpm at no load conditions. In addition, the comparison between the dynamic responses in terms of the IM angular speed obtained with the enhanced FOC (blue line) and with the traditional

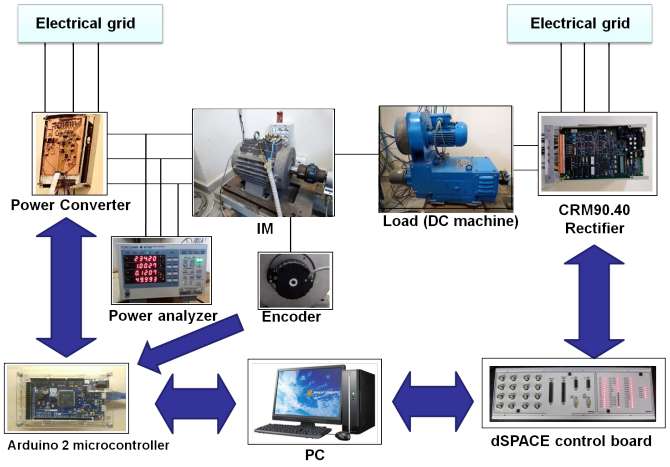


(a)

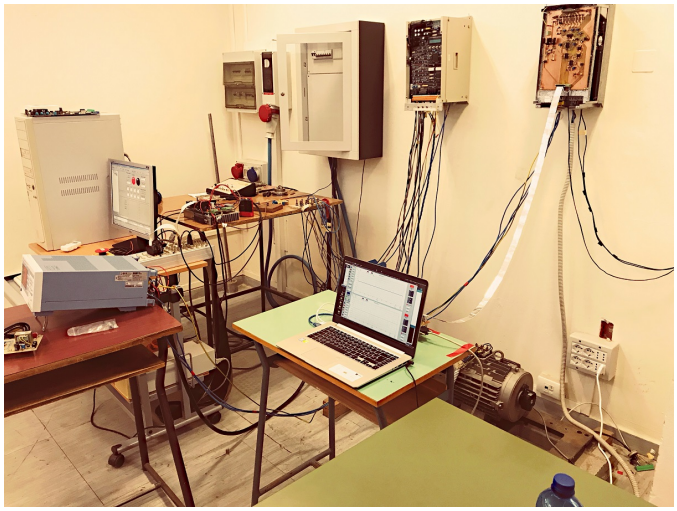

(b)

Figure 4. (a) Schematic representation and (b) a photograph of the test bench

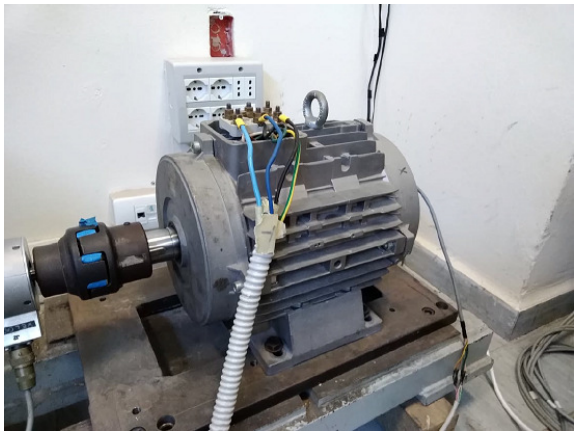

Figure 5. The three-phase induction motor under test.

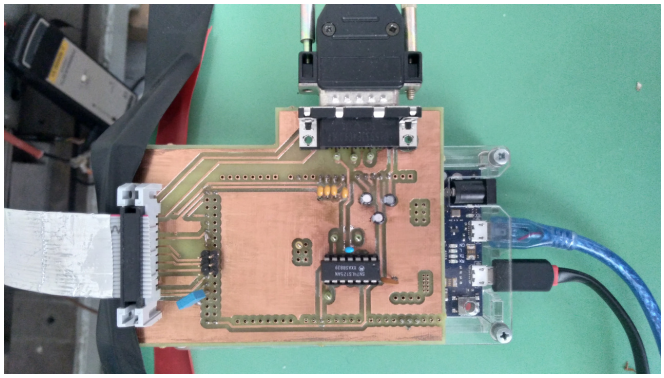

Figure 6. Arduino Due shield.

FOC (red line) for both algorithms are plotted in Fig.12. As well as for the previous cases, it can be noticed that the proposed algorithm provides better dynamic performance.

Besides the results reported in the previous graphs, many working conditions have been examined by adequately setting the torque value of the DC machine (through the dSPACE user interface) and by setting the values of IM flux and mechanical speed through the Arduino board. The experimental results demonstrate the faster transient response of the enhanced technique and its overall higher performances with respect to the traditional FOC strategy.

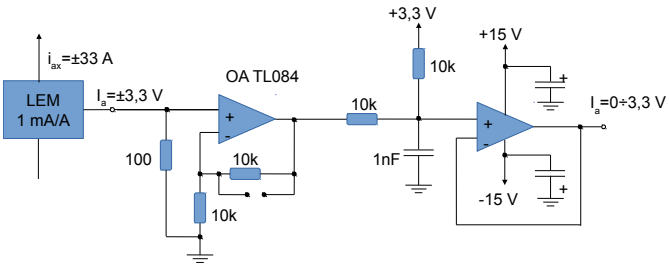


Figure 7. Simplified scheme of the current signals conditioning network.

## V. Cost and Performance Analysis

This Section discusses about the technical and economical features of the adopted microcontroller, which is shown in Fig. 13, with respect to traditional ones.

Generally, the adoption of MCPUs like Field Programmable Gate Arrays (FPGAs), Digital Signal Processors (DSPs) and Complex Programmable Logic Devices (CPLDs), even if providing high performances, can result in high development costs. On the contrary, the Arduino DUE is the perfect compromise between technical and economic performance for most of the electric drives applications. Firstly, by referring to Table III, it can be noticed that the adopted microcontroller, at present days, is the cheapest solution. Secondly, from Section IV, it appears evident that the ARDUINO DUE provides good dynamic performance of the drive: the high flexibility, the high compilation/execution speed of the code and the low clock frequencies represent other advantages of the adopted microcontroller.

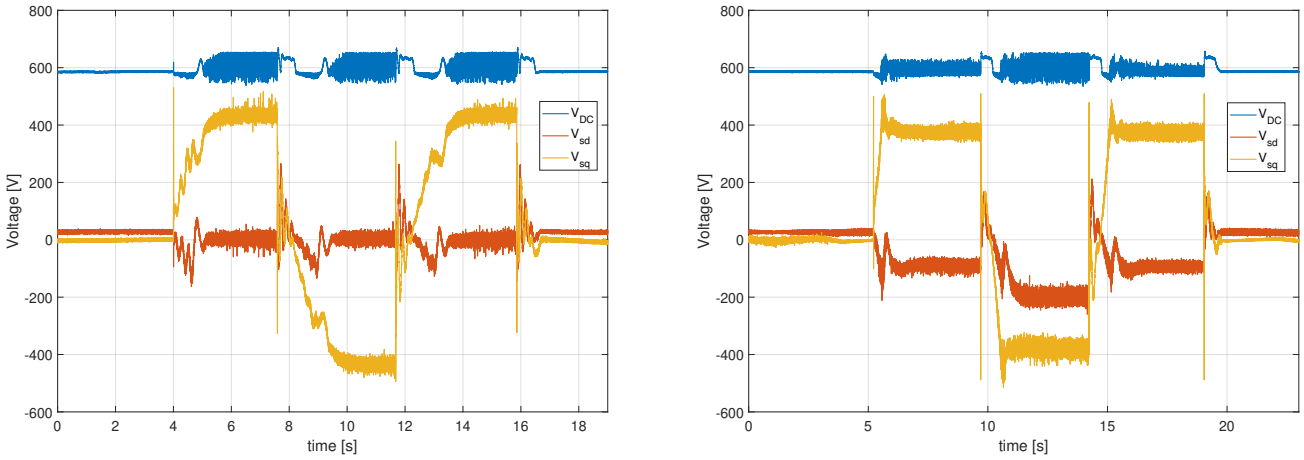


(a) (b)

Figure 8. Experimental results for the implementation of (a) traditional and (b) enhanced FOC algorithms: $V_{sd}$, $V_{sq}$ and $V_{DC}$.

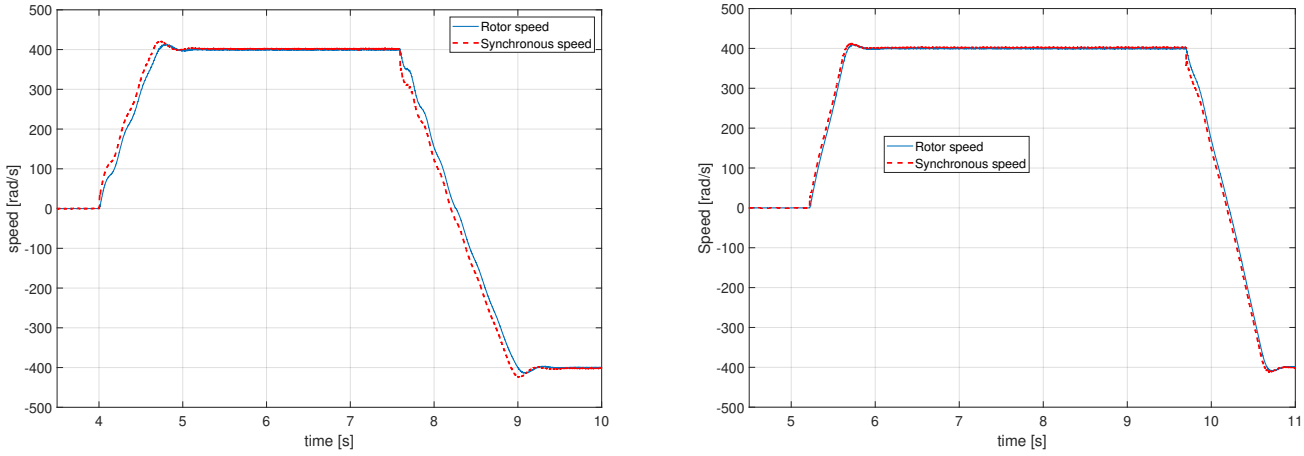


(a) (b)

Figure 9. Experimental results during an acceleration/deceleration test for (a) traditional and (b) enhanced FOC algorithms: $\omega_s$ and $\omega_r$.

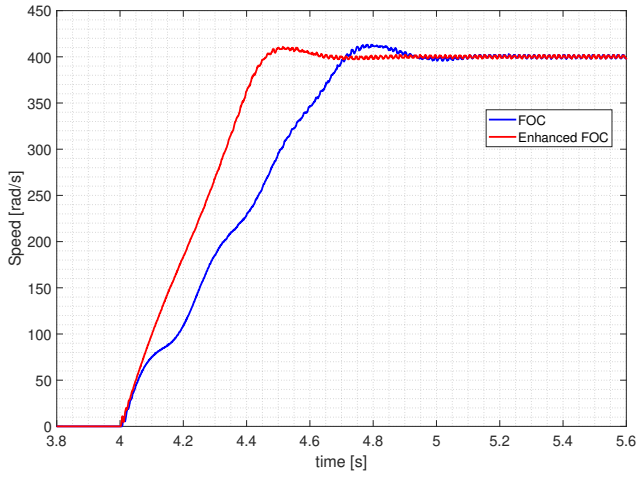


Figure 10. Speed dynamic response comparison between FOC (blue line) and enhanced FOC (red line) algorithms for $\omega_{ref} = 0 \div 400$ [rad/s].

Table III
ECONOMIC ANALYSIS BETWEEN AVAILABLE MICROCONTROLLERS.

| Controller | Model | Freq. MHz | Price USD |
|---|---|---|---|
| Arduino | Arduino DUE | 84 | 38.00 |
| DSP | C2000 controlCARDs-TMS320F2808 | 100 | 61.00 |
| DSP | ADZS-BFSHUSB-EZEXT | 400 | 112.72 |
| DSP | TMDSCNCD28335 control card | 150 | 69.00 |
| DSP | TMDSPREX28335 controlCARD | 150 | 195.00 |
| DSP | TMDSDOCK28069 | 90 | 109.00 |
| FPGA+CPLD | Xilinx® Inc. EK-S6-SP605-G | 1100 | 783.21 |
| FPGA | Xilinx® Spartan®-6 LX4 Digilent Cmod s6 | 133 | 86.00 |
| FPGA | Xilinx® Spartan®-7 Digilent Arty S7-25 | 50 | 99.00 |
| FPGA | Zynq-7000 Xilinx® 7 Cora Z7 | 667 | 99.00 |
| FPGA | DE0-Nano - Altera Cyclone IV | 50 | 99.95 |
| Max V CPLD | Intel DK-DEV-5M570ZN | 247 | 74.90 |

With regard to the technical features, Fig. 14 shows the main flowchart of the software. According to this Figure, the "Hardware set-up" sets the device registers and configures all necessary hardware peripherals. After that, there is the "initialization of the variables". The main loop ("Loop") is sequen-

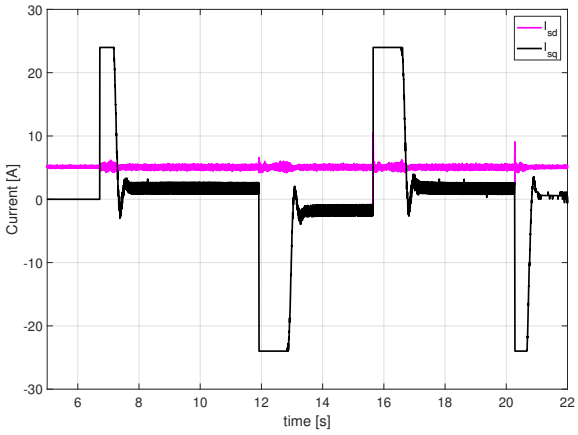


(a)

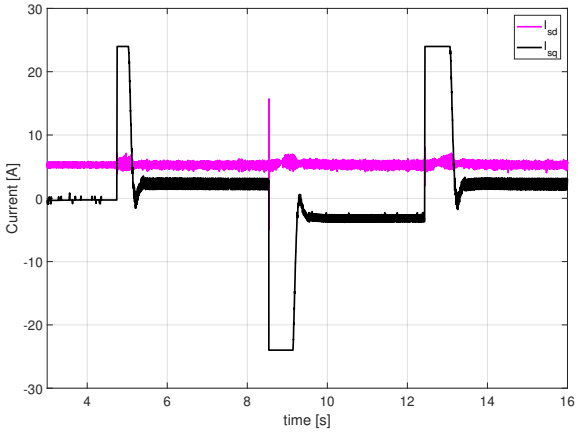


(b)

Figure 11. $I_{sd}$ and $I_{sq}$ profiles during multiple acceleration/deceleration tests for (a) traditional FOC and (b) enhanced FOC.

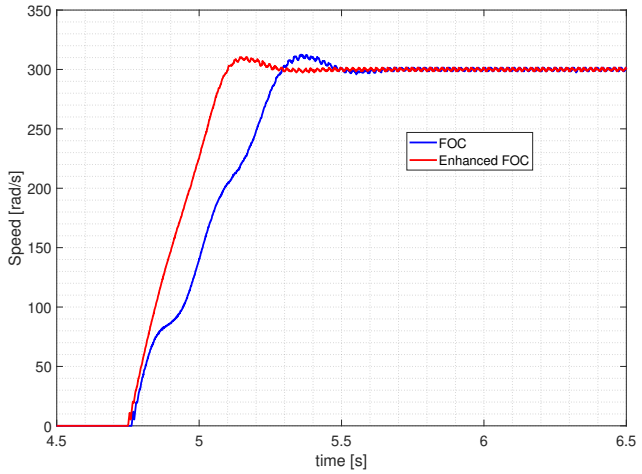


Figure 12. Speed dynamic response comparison between FOC (blue line) and enhanced FOC (red line) algorithms for $\omega_r = 0 \div 300$ [rad/s].

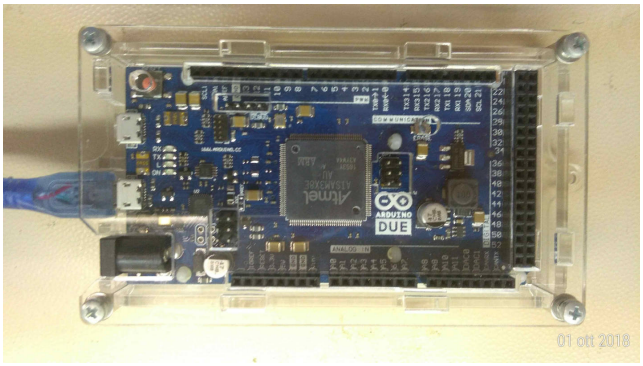

Figure 13. The Arduino Due board.

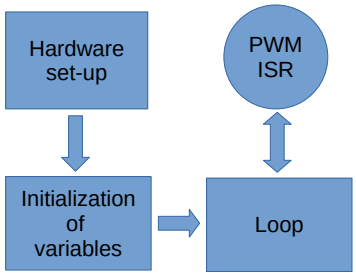


Figure 14. Flowchart of the software.

tially and cyclically processed by the processor following its calculation times; its task is represented by the modification of the reference speed during the working operation of the drive, which occurs via PC serial communication and the reading of 8 real time signals, which can be chosen in by software. The core of the process is represented by three functions: main program, containing the loop and ISRs (Interrupt Service Routines) [24], which trigger the execution of a code section when the processor calls the occurring of a specific event (the ISRs are triggered by the peripherals of the ARDUINO DUE). The PWM_Handler represents the interrupt triggered function and it executes all the process of Fig. 3, including the control equations of Section II and the reading of ADC registers.

By referring to Fig. 15, the interrupt condition occurs at each end of modulation period, determined from the configuration of specific PWM counters, allowing the determination of the PWM period. The related resolution is set at $4096 = 2^{12}$, determining a modulation frequency equal to $f_s = {}^{84000000}/_{2 \cdot 4096} \approx 10254$ Hz and a period of $T_s \approx 97.5$ $\mu$s. This value is adequate with the sine table resolution (12 bit) for the implementation of the transformation matrices. Finally, the phase currents are acquired, at each peak of the PWM counter (i.e. in the middle of the PWM period as shown in Fig. 15), from two hall sensors of the inverter and provides the ABC-$\alpha\beta$-dq transformations.

Another advantage of the Arduino platform is represented by the open-source and easily programmable IDE (Integrated Development Environment), which improves the flexibility and reduces at the same time the set-up time and cost. In conclusion, it can be stated that the used microcontroller is the cheapest solution and it does not affect in a considerable manner the performance of the proposed drive.

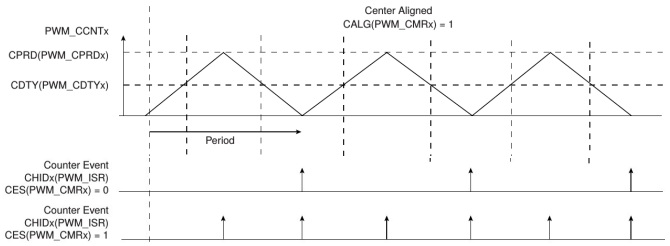


Figure 15. PWM period determination and interrupt signals setup [25].

## VI. Conclusions

This paper has presented an experimental low-cost implementation of an enhanced field oriented control algorithm by adopting the ATSAM3X8E microcontroller, which can be a good compromise between costs and dynamic performance. The experimental results have been compared with those obtained by adopting a FOC algorithm without considering the non linearity behavior of the motor. The user friendly interface has allowed a simple and flexible implementation of the IM drive, without affecting the dynamic performance of the proposed system.

## ACKNOWLEDGMENTS

This work was financially supported by PON R&I 2015-2020 "Propulsione e Sistemi Ibridi per velivoli ad ala fissa e rotante – PROSIB", CUP no:B66C18000290005, by H2020-ECSEL-2017-1-IA-two-stage "first and european sic eight-inches pilot line-REACTION", by Prin 2017- Settore/Ambito di intervento: PE7 linea C - Advanced power-trains and -systems for full electric aircrafts, by PON R&I 2014-2020 - AIM (Attraction and International Mobility), project AIM1851228-1 and by ARS01_00459-PRJ-0052 ADAS+ "Sviluppo di tecnologie e sistemi avanzati per la sicurezza dell'auto mediante piattaforme ADAS".

## References

[1] M. Caruso, V. Castiglia, A. Del Pizzo, R. Miceli, M. Salles, G. Schettino, V. Traversa, and F. Viola, "Low-cost smart energy managment based on atmega 328p-pu microcontroller," in *2017 IEEE 6th International Conference on Renewable Energy Research and Applications (ICRERA)*, pp. 1204–1209, Nov 2017.

[2] M. Caruso, A. O. Di Tommaso, R. Miceli, C. Nevoloso, C. Spataro, and F. Viola, "Interior permanent magnet synchronous motors: Impact of the variability of the parameters on their efficiency," in *2016 IEEE International Conference on Renewable Energy Research and Applications (ICRERA)*, pp. 1163–1167–, Nov 2016.

[3] M. Caruso, A. O. Di Tommaso, R. Miceli, and C. Spataro, "Experimental study on efficiency enhancement in interior permanent magnet synchronous machines," in *2015 International Conference on Clean Electrical Power (ICCEP)*, pp. 518–522, June 2015.

[4] G. Agnello, M. Caruso, V. D. Dio, R. Miceli, C. Nevoloso, and C. Spataro, "Speed control of tubular linear induction motors for industrial automated applications," in *2016 IEEE International Conference on Renewable Energy Research and Applications (ICRERA)*, pp. 1196–1201, Nov 2016.

[5] M. Caruso, G. Cipriani, V. D. Dio], R. Miceli, and C. Nevoloso, "Experimental characterization and comparison of tlim performances with different primary winding connections," *Electric Power Systems Research*, vol. 146, pp. 198 – 205, 2017.

[6] F. Viola, P. Romano, R. Miceli, C. Spataro, and G. Schettino, "Technical and economical evaluation on the use of reconfiguration systems in some eu countries for pv plants," *IEEE Transactions on Industry Applications*, vol. 53, no. 2, pp. 1308–1315, 2017.

[7] F. Pellitteri, G. Ala, M. Caruso, S. Ganci, and R. Miceli, "Physiological compatibility of wireless chargers for electric bicycles," in *2015 International Conference on Renewable Energy Research and Applications (ICRERA)*, pp. 1354–1359, 2015.

[8] A. O. Di Tommaso, R. Miceli, G. R. Galluzzo, and M. Trapanese, "Efficiency maximization of permanent magnet synchronous generators coupled coupled to wind turbines," in *2007 IEEE Power Electronics Specialists Conference*, pp. 1267–1272, 2007.

[9] M. Caruso, A. O. Di Tommaso, A. Imburgia, M. Longo, R. Miceli, P. Romano, G. Salvo, G. Schettino, C. Spataro, and F. Viola, "Economic evaluation of pv system for ev charging stations: Comparison between matching maximum orientation and storage system employment," in *2016 IEEE International Conference on Renewable Energy Research and Applications (ICRERA)*, pp. 1179–1184, 2016.

[10] G. Schettino, C. Buccella, M. Caruso, C. Cecati, V. Castiglia, R. Miceli, and F. Viola, "Overview and experimental analysis of mc spwm techniques for single-phase five level cascaded h-bridge fpga controller-based," in *IECON 2016 - 42nd Annual Conference of the IEEE Industrial Electronics Society*, pp. 4529–4534, 2016.

[11] M. Caruso, A. O. D. Tommaso, F. Genduso, R. Miceli, and G. R. Galluzzo, "A general mathematical formulation for the determination of differential leakage factors in electrical machines with symmetrical and asymmetrical full or dead-coil multiphase windings," *IEEE Transactions on Industry Applications*, vol. 54, no. 6, pp. 5930–5940, 2018.

[12] G. Schettino, S.Benanti, C. Buccella, M. Caruso, V. Castiglia, C.Cecati, A.O.Di Tommaso, R.Miceli, P. Romano, and F. Viola, "Simulation and experimental validation of multicarrier pwm techniques for three-phase five-level cascaded h-bridge with fpga controller," *International Journal of Renewable Energy Research*, vol. 7, no. 3, pp. 1383–1394, 2017.

[13] F. Fernandez-Bernal, A. Garcia-Cerrada, and R. Faure, "Model-based loss minimization for dc and ac vector-controlled motors including core saturation," *IEEE Transactions on Industry Applications*, vol. 36, pp. 755–763, May 2000.

[14] D. Spirov, "Optimal algorithms for minimizing of active and reactive power of induction motors taking into account of iron losses," in *2019 16th Conference on Electrical Machines, Drives and Power Systems (ELMA)*, pp. 1–4, June 2019.

[15] A. M. Bazzi and P. T. Krein, "Review of methods for real-time loss minimization in induction machines," *IEEE Transactions on Industry Applications*, vol. 46, pp. 2319–2328, Nov 2010.

[16] S. Sujitjorn and K. L. Areerak, "Numerical approach to loss minimization in an induction motor," *Applied Energy*, vol. 79, no. 1, pp. 87–96, 2004.

[17] G. Mino-Aguilar, J. M. Moreno-Eguilaz, B. Pryymak, and J. Peracaula, "An induction motor drive including a self-tuning loss-model based efficiency controller," in *2008 Twenty-Third Annual IEEE Applied Power Electronics Conference and Exposition*, pp. 1119–1125, Feb 2008.

[18] T. Stefanski and S. Karys, "Loss minimisation control of induction motor drive for electrical vehicle," in *Proceedings of IEEE International Symposium on Industrial Electronics*, vol. 2, pp. 952–957 vol.2, June 1996.

[19] C. Mademlis, I. Kioskeridis, and T. Theodoulidis, "Optimization of single-phase induction motors-part i: maximum energy efficiency control," *IEEE Transactions on Energy Conversion*, vol. 20, pp. 187–195, March 2005.

[20] Ming-Fa Tsai and Hsien-Chang Chen, "Design and implementation of a cpld-based svpwm asic for variable-speed control of ac motor drives," in *4th IEEE International Conference on Power Electronics and Drive Systems. IEEE PEDS 2001 - Indonesia. Proceedings (Cat. No.01TH8594)*, vol. 1, pp. 322–328 vol.1, Oct 2001.

[21] J. Lin, K. W. E. Cheng, Z. Zhang, and X. Xue, "Experimental investigation of in-wheel switched reluctance motor driving system for future electric vehicles," in *2009 3rd International Conference on Power Electronics Systems and Applications (PESA)*, pp. 1–6, May 2009.

[22] D. Luczak, "Dsp implementation of electric drive control system," in *2012 8th International Symposium on Communication Systems, Networks Digital Signal Processing (CSNDSP)*, pp. 1–3, July 2012.

[23] R. K. Pongiannan and N. Yadaiah, "Fpga based space vector pwm control ic for three phase induction motor drive," in *2006 IEEE International Conference on Industrial Technology*, pp. 2061–2066, Dec 2006.

[24] V. Castiglia, P. Ciotta, A. O. Di Tommaso, R. Miceli, and C. Nevoloso, "High performance foc for induction motors with low cost atsam3x8e microcontroller," in *2018 7th International Conference on Renewable Energy Research and Applications (ICRERA)*, pp. 1495–1500, 2018.

[25] ATMEL, "Sam3x / sam3a series atmel smart arm-based mcu," in *DATASHEET*, pp. 1–1459, Mar 2015.